Palaeogeography, Palaeoclimatology, Palaeoecology 582 (2021) 110641

Contents lists available at ScienceDirect

Palaeogeography, Palaeoclimatology, Palaeoecology

journal homepage: www.elsevier.com/locate/palaeo

Incorporating lateral variability and extent of paleosols into proxy uncertainty

Rebecca M. Dzombak, Nikolas C. Midttun, Rebekah A. Stein, Nathan D. Sheldon *

Department of Earth and Environmental Sciences, University of Michigan, Ann Arbor, MI 48109, USA

ARTICLE INFO

Editor: Thomas Algeo

Keywords:
Paleoclimate
Geochemistry
Wyoming
Eocene
Calcium

ABSTRACT

Paleosols (fossil soils) are valuable records of terrestrial climate and environments, and paleosol-based proxies are commonly used to reconstruct past climates and ecosystems. Results from relatively small outcrops or transects or from single vertical sections are frequently scaled up to represent basin-scale processes and conditions, and reconstructions are relied on for temporal changes in those basins. However, uncertainty arising from limited outcrop extent is not currently considered in the standard application of paleosol-based proxies. To explore uncertainty arising from lateral paleosol heterogeneity, we performed a random subsampling analysis on a newly-collected 2.9 km paleosol transect from SW Wyoming, along with two previously-published paleosols. We demonstrate the importance of sampling multiple paleosol profiles, considering lateral geochemical variability, and focusing on relative rather than absolute changes when outcrop-based uncertainty may require it.

1. Introduction

Paleosols (fossil soils) provide critical, unique insight into the interactions in the 'critical zone' where the atmosphere, biosphere, and geosphere meet at Earth's surface (Brantley et al., 2007; Nordt and Driese, 2014). Because they form at the surface, in constant contact with and in response to regional climates and whatever life is present, paleosols can be used to reconstruct past climates, environments, and chemical conditions of the continents (Jenny, 1941; Harnois, 1988; Maynard, 1992; Cerling, 1984; Rye and Holland, 1998; Retallack, 2001; Sheldon and Tabor, 2009; Sheldon, 2018; Tabor and Myers, 2015). Geochemical proxies derived from soil chemistry are powerful tools for understanding the planet's history, but they remain imperfect. Some baseline limitations for paleosol-based proxies include preservation of their original composition (e.g., Retallack, 1991; Fedo et al., 1995; Rye and Holland, 1998), outcrop exposure, soil order identification (Mack et al., 1993; e.g., Sheldon et al., 2002; Nordt and Driese, 2010; Gallagher and Sheldon, 2013), and their calibration based on modern soil conditions, processes, and datasets. These in turn limit our ability to interpret and extrapolate results beyond the calibration datasets. While the community is continually working to improve paleosol-based proxies, one limitation–outcrop exposure–remains a relatively unaddressed source of statistical uncertainty in paleoclimate reconstructions.

Many paleosol-based proxies are applied to a limited number of paleosol profiles, as determined by outcrop exposure and quality. Because of common proxy development methods and field applications, paleosol-based proxies are not well-constrained at landscape or basin-wide scales, which are often the scales of interest for paleoclimate and paleoenvironmental reconstruction. The field is left with a number of uncertainty sources in these proxies based on outcrop exposure and extent that are not taken into consideration when interpreting results. The ultimate effect of this omission is an overstatement of certainty.

While statistical uncertainty in paleosol-based proxies could be improved in several ways (e.g., focusing on improvements in the calibration datasets and moving away from fixed standard error as in Lukens et al. (2019)), lateral variability in paleosols' geochemistry is one of the key targets for improvement. Modern landscapes host varied microclimates, vegetation, hydrology, and sedimentary architectures, leading to geochemical variability. The same can be assumed to be true for ancient landscapes following the advent of land plants. Sampling practices are inherently limited by outcrop exposure, but no one has yet quantified or demonstrated how this limitation should affect the certainty of paleosol-based climate reconstructions. If, for example, a paleosol has a 50 m laterally-continuous exposure and three profiles are sampled, how should the statistical uncertainty of those paleoclimate reconstructions be treated as opposed to if ten profiles were sampled in that same

* Corresponding author.
E-mail addresses: rdzombak@umich.edu (R.M. Dzombak), nmidttun@umich.edu (N.C. Midttun), restein@umich.edu (R.A. Stein), nsheldon@umich.edu (N.D. Sheldon).

https://doi.org/10.1016/j.palaeo.2021.110641
Received 6 March 2021; Received in revised form 9 July 2021; Accepted 29 August 2021
Available online 6 September 2021
0031-0182/© 2021 Elsevier B.V. All rights reserved.

section? How large a lateral exposure, or multiple exposures, should be used to represent basin-wide climate or ecosystems? At a fundamental level, the base geochemical variability within a paleosol outcrop should be considered as part of proxy uncertainty, rather than relying solely on the fixed proxy error, but this is not currently standard practice.

Some previous work has considered lateral variability in paleosol-based proxies, such as Kraus (1999) and Hyland and Sheldon (2016), which focused on quantifying sedimentological and geochemical variability in paleosols at km-scale, respectively. Kraus' work in the 1980s and 1990s pushed forward the concept of pedofacies and soils' spatial relationships with basin-wide sedimentological processes (Bown and Kraus, 1987; Kraus, 1997; Kraus, 1999). Hyland and Sheldon (2016) found that geochemical variability across a 1 km single-paleosol transect of the Wasatch Fm. was relatively low and proxies were reliable. Similarly, Stiles et al. (2001) found no lateral variability within a single pedon for their Fe nodule-based MAP reconstruction. Driese and Ashley (2016) sampled four paleosols with <1 km of each other and found geochemical consistency. More work exists constraining the variability of paleosol types and environmental variability within a basin in a tectonic/sedimentological context (see Tabor and Myers, 2015). Tabor et al. (2006) examined general paleosol variability (not a single paleosol transect) across 15 km in the Ischigualasto-Villa Union basin in Argentina, where they found uneven paleosol distributions and thicknesses derived from geomorphic heterogeneity, as well as variability in the pedogenic carbonates' oxygen isotope values. Rosenau et al. (2013a, 2013b) observed basin-scale variability in paleosol type, linked primarily to the degree of marine influence. Thus, while a number of studies have examined lateral paleosol variability as a first step towards considering local environmental variability. Here we identify an opportunity for proxy improvement by explicitly quantifying how lateral variability translates to certainty or uncertainty in proxy reconstructions.

Additional efforts for improving the treatment of uncertainty have included developing proxies based on individual soil orders and soil functional types, which is critical because different soils have distinct chemical traits/processes (e.g., Sheldon, 2006; Nordt and Driese, 2010; Gallagher and Sheldon, 2013). Several researchers have focused on modifying the statistical treatment of proxies (e.g., Breecker, 2013; Stinchcomb et al., 2016; Lukens et al., 2019). For pedogenic carbonate-based proxies, understanding what part of the year a proxy represents has been shown to be critical for accurate interpretation of carbon and oxygen isotopes (Passey et al., 2010; Gallagher and Sheldon, 2016; Gallagher et al., 2019a; Gallagher et al.,2019b; Kelson et al., 2020) and different workers have also improved the interpretation of carbonate isotope geochemistry by using both inorganic and organic isotopes (Tabor et al., 2013; Tabor et al., 2017; Sheldon, 2018). Constraining lateral geochemical variability in paleosols provides essential background information for each of those techniques and the methods discussed in this work could easily be applied to other approaches (e.g., C isotopes in organic matter, pedogenic carbonate) and likely has implications for the taphonomy of phytoliths as well (e.g., Hyland, 2014).

The presence of pedogenic carbonates, whether authigenic or diagenetic, can strongly influence many paleosol-based proxies, to the point that some proxies define acceptable levels of carbonate (e.g., Sheldon et al., 2002; Nordt and Driese, 2010; Michel et al., 2016). Authigenic pedogenic carbonate is linked to precipitation and soil saturation, with proxies such as depth to Bk horizon relying on that relationship (Jenny, 1941; Retallack, 2005). Secondary or diagenetic carbonate, which does not reflect original soil formation conditions, can therefore skew paleosol proxy results (e.g., Retallack, 1991; Michel et al., 2021). Treatment of samples, either in sample preparation or processing/analysis, can also affect Ca concentrations and therefore impact proxy-based reconstructions (Michel et al., 2021). For example, with the CIA-K precipitation proxy, an anomalously high Ca concentration leads to an underestimation of precipitation; the accidental removal of authigenic carbonate through non-conservative pre-treatment (such as 20% H_2O_2), on the other hand, would lead to overestimating precipitation (Michel et al., 2021). Therefore, paleosol Ca content merits careful consideration, particularly in the context of spatial variability and the representativeness of any given paleosol profile.

By quantifying baseline geochemical heterogeneity and testing the robustness of select paleosol-based proxies at basin scales, ideally at multiple sites in a range of environments and soil orders, we can improve our understanding of km-scale processes in paleosols, make our proxies more statistically robust, and ultimately strengthen certainty in basin-wide paleoclimate and paleoenvironment reconstructions. Basins with good exposure and relatively flat-lying, continuous terrestrial strata are ideal testing grounds for the effects outcrop extent have on proxy uncertainty. Here, we examine the lateral variability of two Eocene paleosol transects and make a first attempt at quantifying the magnitude of uncertainty associated with km-scale outcrop resampling.

2. Field site and geologic context

With its flat-lying deposits, ample exposures, and high-resolution age constraints, the Eocene Green River Basin in SW Wyoming, USA (Fig. 1) has been the subject of many paleoclimate and paleoenvironmental studies, including some previous work on lateral geochemical variability (e.g., Hyland and Sheldon, 2016). These strata record a lacustrine to fluvial floodplain environment during a relatively warm and wet period and span the early Eocene climatic optimum (EECO; Braunagel and Stanley, 1977; Clyde et al., 1997; Clyde et al., 2001; Smith et al., 2008). The basin received sediment inputs from the proximal Wind River Range during the Eocene (Chetel and Carroll, 2010; Hyland and Sheldon, 2013) and is relatively well-dated due to stratigraphic correlation to dated tuffs, paleomagnetic records, and land mammal stratigraphy (Clyde et al., 2001; Smith et al., 2008). The floodplain deposits outside of paleo-Lake Gosiute are represented in part by the Eocene Wasatch Formation. These laterally-extensive outcrops are striking red, orange, yellow, and purple stripes on the tan-to-white backdrop of lacustrine deposits and stretch across basins, making them ideal targets for testing lateral heterogeneity and constraining statistical uncertainty in proxies.

Within the Wasatch Fm. of Wyoming, we focus on two sites of approximately the same age: previously sampled paleo-Alfisols of Honeycomb Buttes (HB; 42.237°N, 108.533°W, as reported), the site of Hyland and Sheldon (2016)'s work, and the new site presented here, Jack Morrow Hills (JMH), which is characterized by paleo-Inceptisols. The two sites are ca. 35 km apart (Fig. 1). The JMH transect is within the Main Body of the Wasatch Fm. and is overlain by the Tipton Member of the Green River Fm. (Sutherland and Luhr, 2011). The excellent exposures at JMH and HB are thanks in part to their position within the uplifted and incised northern extent of the Laramide-age Rock Springs Uplift (Mederos et al., 2005). Physically, they differ primarily in apparent redox condition: while Honeycomb Buttes is dominated by red-orange paleosols (oxidized), the JMH transect quickly transitioned from red-orange to dominantly purple (reduced) paleosols with grey, green, and yellow reduction mottles. Because of this difference, comparing the resampling results between the two sites is informative of broad soil conditions (i.e., not limited to either reduced or oxic paleosol or to a single soil order).

3. Methods

3.1. Access and sampling

The Jack Morrow Hills (JMH) transect (42.104°N, 109.055°W; ca. 2225 m) is located in Sweetwater County, WY, north of Jack Morrow Creek in the broader Antelope Hills area (Fig. 1). It is federal land managed by the BLM. It was accessed off of Hwy 28 between Farson and South Pass City, via county roads 21 and 83.

A lateral transect of a continuous paleosol was followed over 2.9 km,

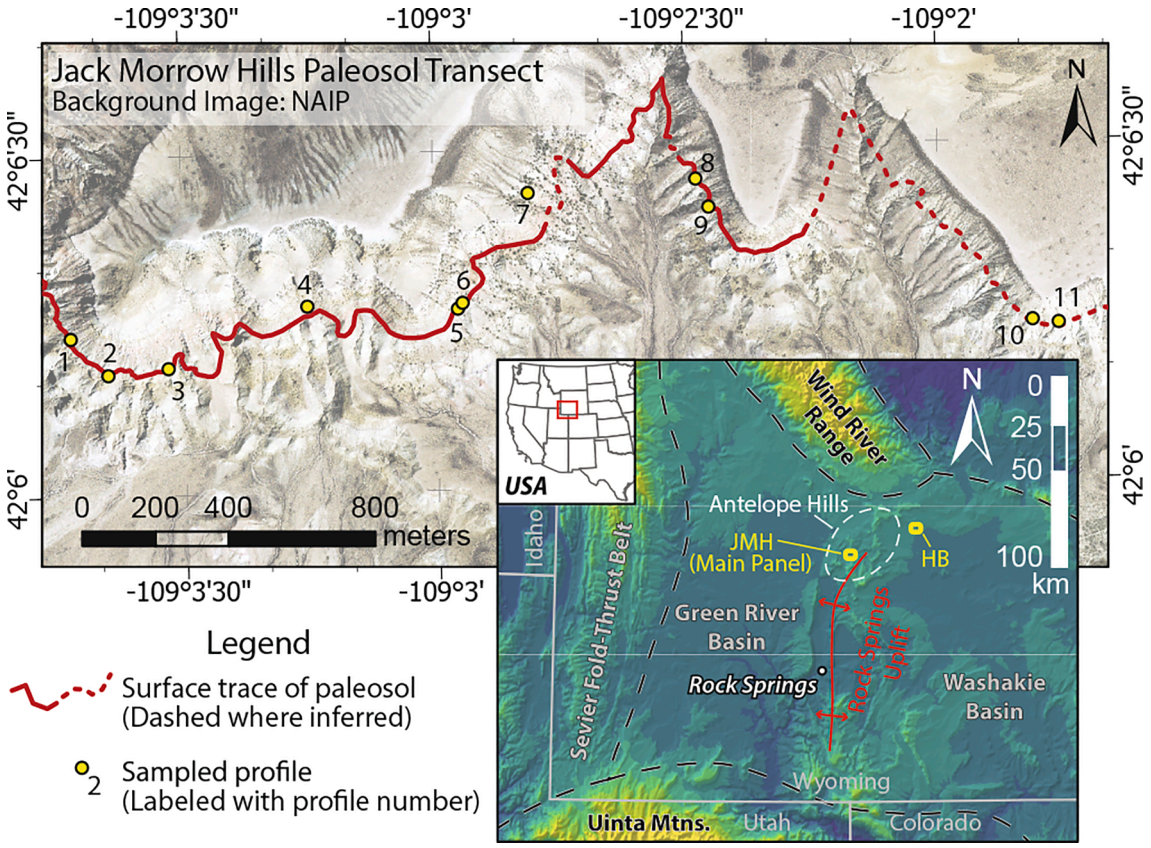

Fig. 1. Map of sampling locations. JMH = Jack Morrow Hills (new paleosols in this work), HB=Honeycomb Buttes (Hyland and Sheldon, 2016). Lower panel shows regional geography, with the two sampling sites marked in yellow nearby the Rock Springs Uplift (red lines). Top panel shows the JMH paleosol transect; yellow dots mark sampled paleosol profiles. Dashed red line indicates inferred trace due to access limitation (e.g., too steep or too vegetated to reach). (For interpretation of the references to color in this figure legend, the reader is referred to the web version of this article.)

identified by its stratigraphic position above interspersed thick channel deposits and as part of a two-paleosol couplet (Fig. 2). Within the transect, ten profiles were sampled, and one profile was sampled from an overlying paleosol (red star in Fig. 3; Paleosol 7 in Fig. 4). At each profile, trenches (at least ca. 20 cm deep) were dug until fresh rock, unaffected by modern surface processes, was reached. Modern vegetation and roots were avoided during sampling. Within each profile, samples were taken to represent each color or horizon change, and multiple samples within most B horizons to ensure intra-horizon replicability of results. One stretch of the transect (2–3 km) had steep slopes and more vegetation, so we were unable to sample the paleosol at the ca. 2.5 km mark. After ~3 km, the paleosol couplet became less distinct and the butte was more eroded, effectively limiting the transect length to ca. 3 km. Sample locations and descriptions are found in Table S1.

3.2. Sample preparation and analysis

Samples were crushed in a Shatterbox, dried at room temperature, and ground to <2 μm. Samples were not acidified in order to preserve Ca content. Bulk geochemistry was performed at ALS Minerals in Vancouver, BC via conservative four-acid digestion and ICP-MS analysis. Instrument error is <0.01% for major elements. Bulk geochemical data are reported in Table S2; extended CaO data are in Table S3.

3.3. Proxies

To test paleoclimate reconstructions, we used the Chemical Index of Alteration minus potash (CIA—K; Harnois, 1988; Maynard, 1992)-derived mean annual precipitation (MAP) proxy (Sheldon et al., 2002; Sheldon and Tabor, 2009). CIA-K is calculated on a molar basis following Eq. 1, and MAP from CIA-K in Eq. 2. The error for CIA-K-based MAP, ±182 mm yr^{-1}, is the standard error of the regression from Sheldon et al. (2002).

$$\text{CIA} - \text{K equation } Al_2O_3/(Al_2O_3 + CaO + Na_2O) \quad (1)$$

$$\text{MAP equation } MAP = 221e^{0.0197(CIA\ \ K)},\ \pm 182 \text{ mm yr}^{-1} \quad (2)$$

To test our resampled uncertainty on an unrelated paleosol, we also included in our statistical analysis a previously-sampled ~1.5 km Vertisol paleocatena from Kenya (Kisaaka; reported as ca. 0.84°S, 34.15°E, ca. 1170 m) which, with only 4 profiles' bulk geochemistry available over that distance but robust intra-paleosol sampling, provides a good point of comparison (Beverly et al., 2015, 2017). Because that transect contained Vertisols, we used the CALMAG MAP proxy, which was calibrated on and intended for application on Vertisols (Nordt and Driese, 2010). CALMAG is similar to other Al/base cation ratios but includes CaO and MgO, as the two cations with the strongest correlations with MAP (Nordt and Driese, 2010) rather than Na_2O and CaO (e.g., CIA—K). While some users have treated the CIA-K and CALMAG proxies as interchangeable, CALMAG would be inappropriate for quantitative use with JMH and HB paleosols (Inceptisols/Alfisols). Instead, we use a comparison between proxies to consider the role of paleosol taxonomy in increasing or decreasing reconstruction uncertainty.

$$\text{CALMAG} = Al_2O_3/(Al_2O_3 + CaO + MgO) \times 100 \quad (3)$$

$$MAP_{CM} = 22.69\text{xCALMAG}–435.8, \text{RMSE} = \pm 108 \text{ mm yr}^{-1} \quad (4)$$

Additionally, we checked two mean annual air temperature (MAAT) proxies (SAL, PWI) for lateral continuity (Fig. S1) (Retallack, 1991; Sheldon et al., 2002; Gallagher and Sheldon, 2013). To test for intra- and

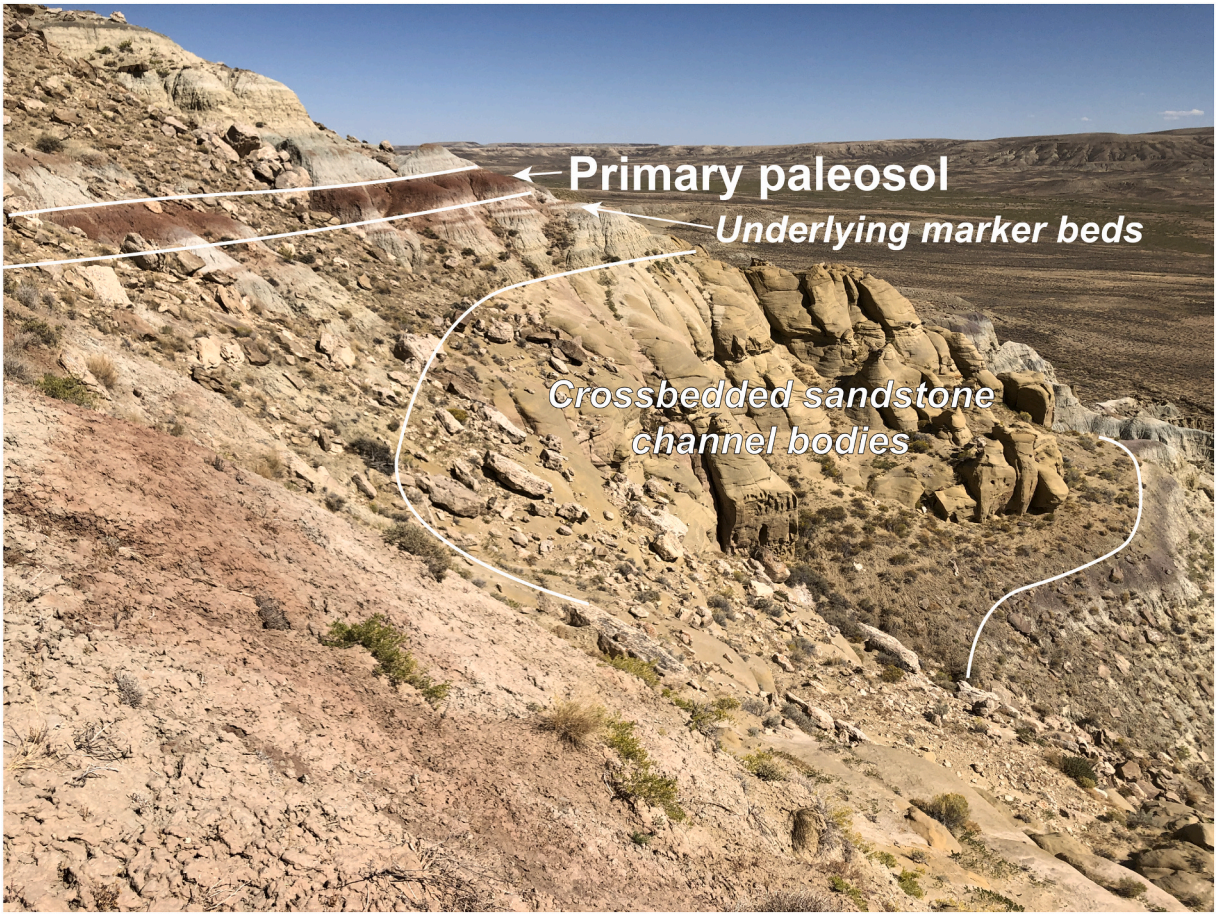

Fig. 2. Full JMH section in profile, with massive fluvial sandstone underlying stacked paleosol successions. The distinctive paired dark-red paleosols were present for nearly 3 km, despite a transition from red to purple dominant hue. Channel sandstones were intermittently present at the same relative stratigraphic level. (For interpretation of the references to color in this figure legend, the reader is referred to the web version of this article.)

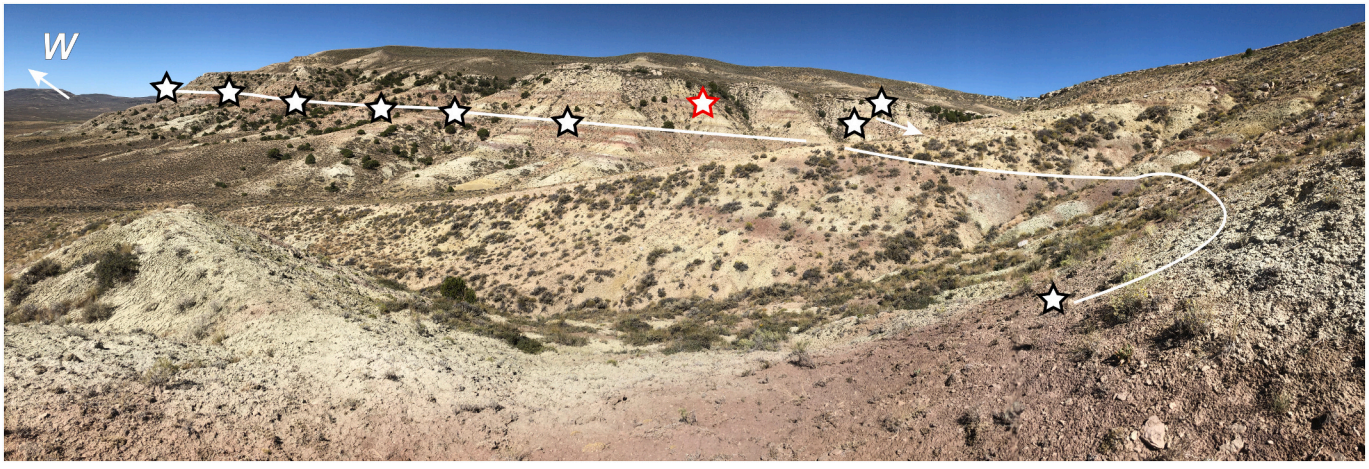

Fig. 3. JMH site overview, with sampling locations marked by stars. Red star indicates a profile (#7) accidentally sampled from overlying paleosol. (For interpretation of the references to color in this figure legend, the reader is referred to the web version of this article.)

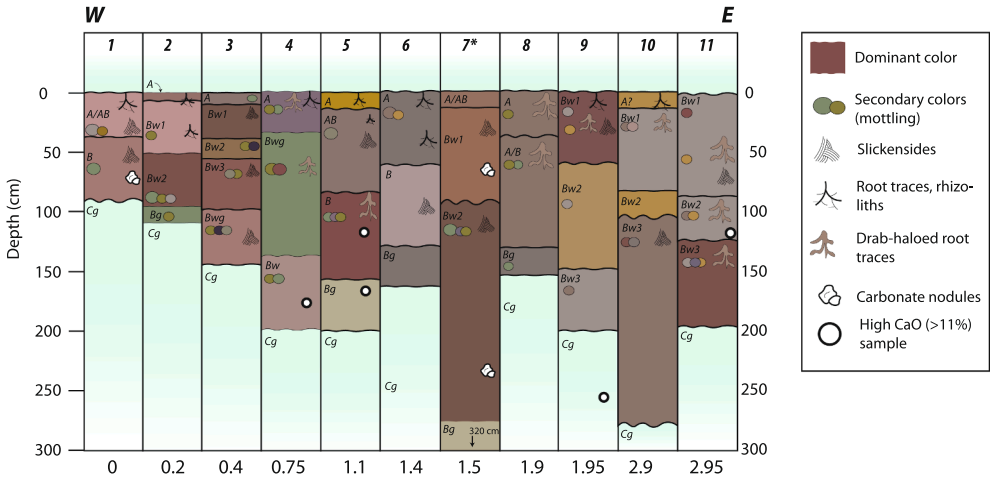

Fig. 4. Cartoon of each JMH paleosol profile, from W to E (left to right). A general shift from oxic to reducing conditions is apparent based on paleosol color, as well as an increase in profile thickness. Along with a decrease in channel sandstones on the eastern end of the transect, this change could reflect more distal, ponded conditions. Carbonates and rootlets were sparse across the transect, with slickensides as the most common pedogenic feature.

inter-paleosol geochemical variability, MAP and MAAT proxies were explored both within single profiles and across the transect.

$$\mathrm{PWI} = [(4.20 \times \mathrm{Na}) + (1.66 \times \mathrm{Mg}) + (5.54 \times \mathrm{K}) + (2.05 \times \mathrm{Ca})] \times 100 \quad (5)$$

$$\mathrm{MAAT_{PWI}} = -2.74\, ln(\mathrm{PWI}) + 21.39, \mathrm{SE\ of\ regression} = \pm 2.1^{\circ}\mathrm{C} \quad (6)$$

$$\mathrm{SAL} = (\mathrm{K_2O} + \mathrm{Na_2O})/\mathrm{Al_2O_3} \quad (7)$$

$$\mathrm{MAAT_{SAL}} = -18.5\mathrm{xSAL} + 17.3, \mathrm{SE\ of\ regression} = \pm 4.4^{\circ}\mathrm{C} \quad (8)$$

Holdridge life zones provide a semi-quantitative means of matching climate with vegetation and provide the underpinnings for other modern approaches to soil energy models (Holdridge, 1947; Lugo et al., 1999). Mean annual precipitation and the ratio of estimated evapotranspiration to MAP (ET/MAP) are plotted on a ternary diagram, with classes (as defined by the International Institute for Applied Systems Analysis) overlaid based on modern vegetation maps. For paleosols, paleo-ET is estimated based on the difference between reconstructed MAP and soil effective precipitation (P_{eff}) (Rasmussen et al., 2005; Rasmussen and Tabor, 2007; Gulbranson et al., 2011). In modern environments, P_{eff} is a linear function of MAP and ET (Gulbranson et al., 2011). This empirically-derived relationship can be used to estimate P_{eff} values for a MAT range of 10–13 °C using Eqs. 9, 10 (Gulbranson et al., 2011):

$$P_{eff} = 0.924(\mathrm{MAP}) - 19.221 \quad (9)$$

and related to ET through Eq. 10 (Gulbranson et al., 2011):

$$\mathrm{ET} = \mathrm{MAP_{CIA-K}} - P_{eff} \quad (10)$$

Data for Holdridge calculations can be found in Table S4.

3.4. Statistical analysis

To demonstrate how the number of profiles sampled can affect paleoclimate reconstruction uncertainty, average MAP values from primarily North American B horizons (which are used for paleoclimate reconstruction due to their longer formation times) were calculated from random subsamples of all profiles from each paleosol horizon. For JMH (profile $n = 11$), the 11 profiles were subsampled in 11 rounds that each used an increasing number of randomly selected profiles, starting with a single profile and ending with all 11 profiles. Each round of subsampling consisted of 10,000 trials, during each of which the average MAP values from the 1–11 randomly selected profiles were recorded. Each of the 10,000 mean values were then nudged by a normally-distributed random value based on standard error of the proxy regression, originally 182 mm yr^{-1} (Sheldon et al., 2002; Prochnow et al., 2006). Because the original reported error is the standard error of the regression, which is approximately similar to 2σ, we nudged the resampled mean by ±91 mm yr^{-1}. Deviation from the mean, as 95% confidence intervals, were also calculated to represent the convergence towards μ + 2σ. The final result of each round of subsampling was a distribution of 10,000 mean MAP values that could result from only using the number of profiles (1−11) prescribed in that round of subsampling and accounting for the proxy error. At HB (profile $n = 10$), resampling used permutations of 1–10 randomly selected profiles, and at Kisaaka paleosol (profile $n = 4$), permutations of 1–4 profiles.

All 11 profiles were included in the JMH resampling regardless of geochemistry or stratigraphic location, to most accurately reflect the possibility of mis-sampling during fieldwork. Resampling tests were repeated with (a) all B-horizon samples, (b) only samples with <5% CaO (Prochnow et al., 2006; Sheldon and Tabor, 2009), and (c) only samples with <11% CaO, a threshold determined by the distribution of CaO in modern Inceptisols as described below. The resampling with samples <5% CaO, as the most conservative proxy, are in main text figures; others are presented in the supplement for comparison. No HB samples fell outside the 5% CaO threshold, so no repeat resampling tests were necessary for those profiles. We also resampled data from the 4 profiles from the Kisaaka paleosols, with a nudge of 108 mm yr^{-1}, the original RMSE. No Kisaaka samples fell outside the 10% CaO limit for CALMAG to be considered applicable.

First, to quantify a baseline for soil CaO concentrations, we used the USGS database of modern soil geochemistry, including A and C horizons and the top 5 cm of the soil, across a range of soil orders (Smith et al., 2014; $n = 4857$). For B horizons, which were not included in the USGS database, we used the Marbut (1935) dataset ($n = 46$), a dataset our lab compiled for previous work (Dzombak and Sheldon, 2020; $n = 195$), and the Vertisol transect used to calibrate CALMAG (Nordt and Driese, 2010). Soil orders included in this Ca analysis are Andisols, Alfisols, Aridisols, Gelisols, Histosols, Inceptisols, Oxisols, Mollisols, Spodosols, Vertisols, and Ultisols, though the resulting dataset is dominated by Mollisols ($n = 60$), Ultisols ($n = 57$), Aridisols ($n = 55$), Alfisols ($n = 44$), and Vertisols ($n = 42$). For all horizons, CaO data are log-normally distributed, with long right tails (Fig. S2, S3). Based on the USGS data, CaO values in the 95th percentile in Top 5 cm/A horizons are about 8.5%, and in C horizons around 14.5% (Table S3). For B horizons, the 95th percentile in all soil orders' CaO was 17% CaO ($n = 325$). The 95th percentile of CaO for modern Inceptisols only (the designation of JMH paleosols) and B horizons only (used for paleoclimate reconstructions) is 11% (Table S3). Both 5% and 11% were used as thresholds for Ca

screening at JMH and HB. To improve Ca screening in paleosols, future work should constrain modern Ca distributions more robustly for each soil order. (This could also improve geochemical paleosol designations.)

Code for subsampling is available in the supplemental materials online at DOI:10.17632/kpdngx4m2f.1.

4. Results

4.1. Paleosol description

Complete descriptive features for each horizon are found in Table S1. Profiles were typically between 1 and 2 m thick with a B and C horizon; A horizons were typically truncated or present as A/AB transitions, denoted primarily by textural changes (e.g., sandy vs. silty/clayey) accompanied by the presence of root traces (Fig. 4). Root traces were sparsely present, and slickensides were pervasive throughout (Fig. 5d). Only two profiles (Paleosols 1 and 7) yielded pedogenic carbonate nodules (Fig. 5e), despite several other profiles having anomalously high Ca concentrations in certain samples (white circles in Fig. 4). Hydromorphic features (e.g., drab-haloed root traces and redoximorphic mottling) were consistently present across the transect. Based on the degree of horizon development but lack of other diagnostic features, the paleosols were identified as paleo-Inceptisols, some with Vertic features (i.e., slickensides). They are designated as paleo-Incepisols rather than

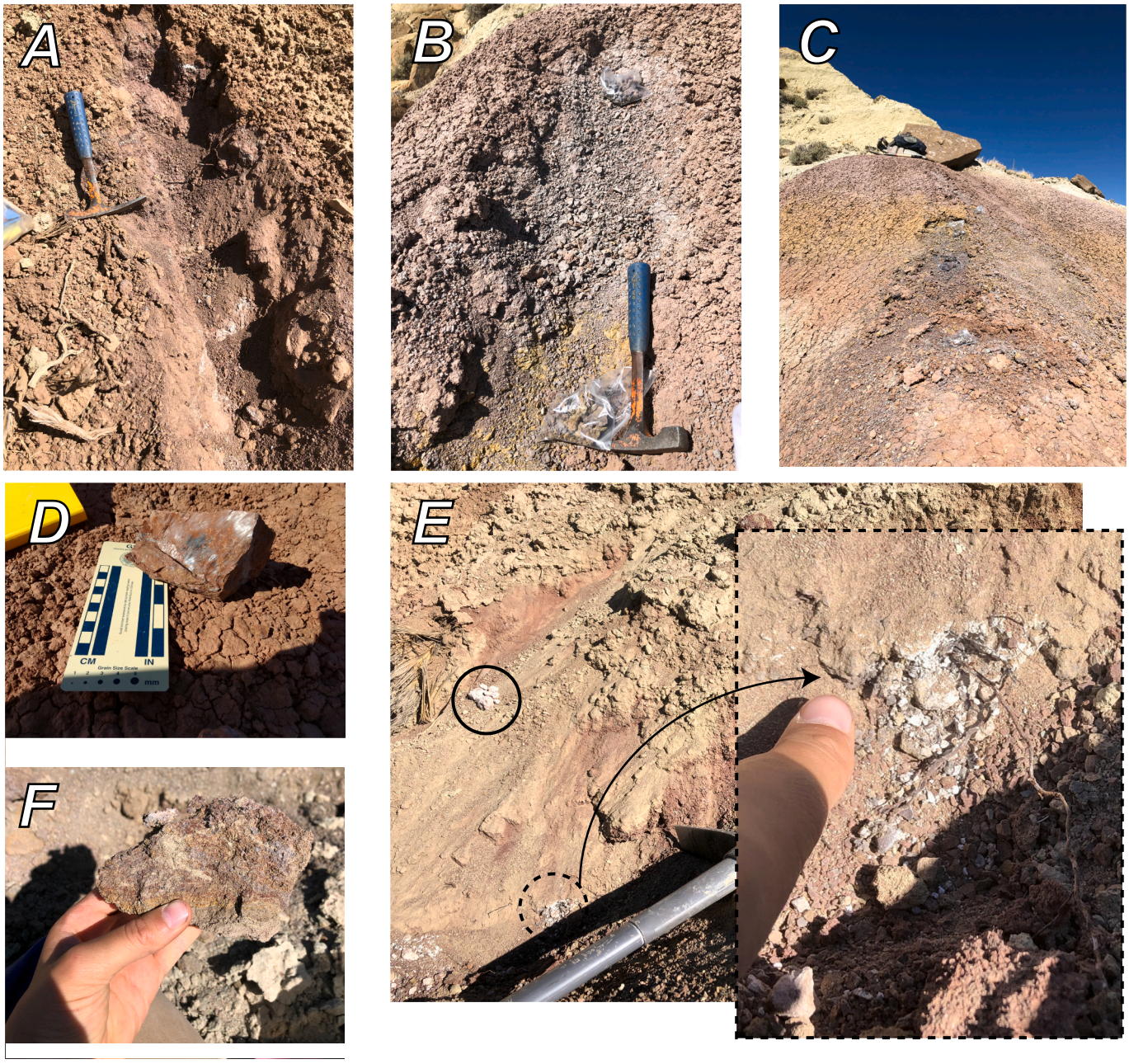

Fig. 5. JMH paleosol profile and detail photos. (A) Trench of oxic paleosol on western end of transect; hammer for scale. (B) Trench of transitional, purple-dominant paleosol; hammer for scale. (C) Trench of far eastern paleosol, with purple, red, and mottled yellow horizons present; backpack and field shovel at top of ridge for scale. (D) Slickenside on paleosol ped. (E) Examples of carbonates, with collected nodules marked with the black circle. Dashed circle and zoomed-in dashed rectangle show modern roots using paleo-carbonate as nutrient hotspot. Because nodules were in float rather than in place, and in-situ carbonate was influenced by modern roots, analyses of carbonates were not possible for this transect. (F) Hand sample of mottled paleosol. (For interpretation of the references to color in this figure legend, the reader is referred to the web version of this article.)

-Alfisols or -Vertisols because no other Vertic features were present and B horizons were not clay-rich enough to qualify as Bt horizons. Paleosol profiles for the complete transect are depicted in Fig. 4. From west to east, the paleosol thickened and changed dominant color scheme, and the interspersed large channel bodies became smaller and sparser.

One profile was mistakenly sampled in the overlying paleosol (Paleosol 7; red star in Fig. 3), but yielded similar geochemical results, providing a temporal/vertical point of comparison.

4.2. Physical and geochemical variability

Across the transect, the primary physical change in the paleosol was a shift from dark red to purple as the dominant color, with reduction mottling and drab-haloed root traces increasing as the paleosol became dominantly purple/grey eastward (Fig. 4). The JMH transect had more color variability than the transect at HB. The sediment distribution also gained some silt in the easternmost samples, but we did not see sandy channels directly interfingered with this particular paleosol at our sampling sites.

Overall, paleosol geochemistry for most elements within paleoclimate proxies (Al, Na, K) was consistent across the transect, despite apparent shifts in redox conditions (color change; Table S2). Redox-sensitive elements (Fe, Cr, Mn) generally showed consistency across the transect, despite a shift from red-orange to purple-dominant claystone (Fig. S4). Down-profile trends in Ti/Al (Fig. S5b) reflect steady, minimal detrital input during soil formation, and down-profile trends in CIA-K (Fig. S5a) reflect typical within-profile weathering patterns (e.g., Sheldon and Tabor, 2009).

However, CaO concentrations did vary notably in several profiles (Paleosols 4, 5, 9, 11 in Fig. 4), despite the absence of obvious sources like pedogenic carbonate nodules or grain coatings. Because these high CaO values directly affected proxy reconstructions, we tested how excluding CaO values above different thresholds would affect the MAP reconstructions for individual profiles (and in resampling, see below). For JMH samples, 10 B-horizon samples exceeded the 5% threshold, and 3 B-horizon samples exceeded the 11% threshold. For HB samples, no B-horizon samples exceeded the 5% CaO threshold. In JMH B horizons, CaO correlates significantly with Mn, but less strongly with Fe and Cr (Fig. S6).

4.3. Proxy variability

Across the transect, MAP and the other indices were bimodally distributed about the mean, with one cluster of values around the mean and another, lower cluster present in paleosols with high Ca values (e.g., Paleosol 4; Fig. 6). Reconstructed MAP values from JMH B horizons averaged 1038 ± 182 mm yr^{-1} with high-CaO samples and 1185 ± 182 mm yr^{-1} excluding high-CaO samples. The magnitude of the increase in mean MAP value is within the standard error of the proxy, making it statistically insignificant. However, the individual MAP values of the high-CaO samples are significantly lower than the mean, with the 5% and 11% threshold samples resulting in reconstructed MAP values from 300 to 500 mm yr^{-1}. This range is statistically significantly different from the overall mean; additionally, such MAP values would represent a different terrestrial biome that is not supported by other paleoclimate and paleoenvironmental work in this region.

For the JMH transect, MAAT reconstructions from B-horizon PWI and SAL averaged 12.7 ± 2.1 and 11.7 ± 4.4 °C, respectively. (Including samples from all horizons lowers those values to 12.6 and 11.5 °C, respectively; the change is within each proxy's error but still demonstrates the effect including the incorrect horizons has on the proxies.) These temperatures are lower than MAATs derived from leaf-margin analysis of several penecontemporaneous Green River Basin early Eocene localities (>20 °C, Wilf, 2000; Fricke and Wing, 2004; Hyland et al., 2018; see Section 5).

Within Holdridge life zone space, each paleosol profile plotted in the wet forest biome with the exception of Paleosol 4, which plotted as a wet tundra (Fig. S7). For comparison, the nearby HB also plotted as wet forest. We plotted the modern southwestern Wyoming climate as a check, and it fell appropriately within the dry scrub biome.

The Kisaaka paleosol had moderate geochemical variability, with two of the four profiles' reconstructed MAP ranges and standard deviations being larger than the others (Fig. S8). As with the JMH paleosols, CaO content is the primary driver of variability across that transect.

4.4. Resampling and statistical constraints

Our random resampling showed that the distribution of MAP reconstructions narrows as more profiles are added to the sampling, with the final iteration (all profiles and samples included) effectively

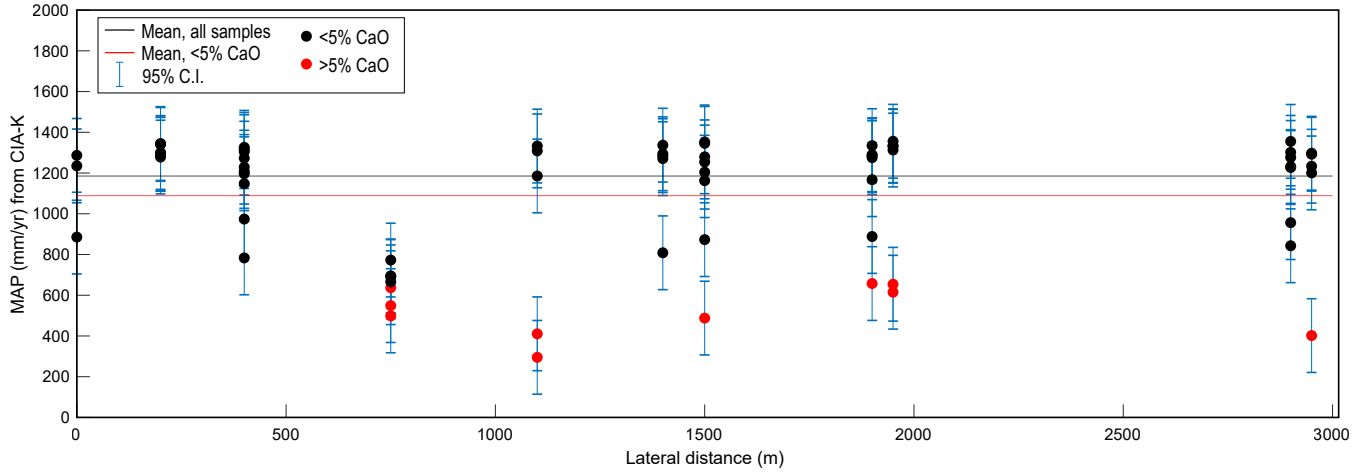

Fig. 6. Lateral variability in MAP reconstructed from CIA—K. Each dot is one B-horizon sample. Black dots are under the 5% CaO threshold, red dots exceed 5% CaO. The error bars are 95% confidence intervals, based on CIA-K regression error. The solid black horizontal line is the average MAP including only samples with CaO <5%; the red horizontal line is the mean including all samples. Excluding samples >5% CaO results in a higher overall average MAP. (For interpretation of the references to color in this figure legend, the reader is referred to the web version of this article.)

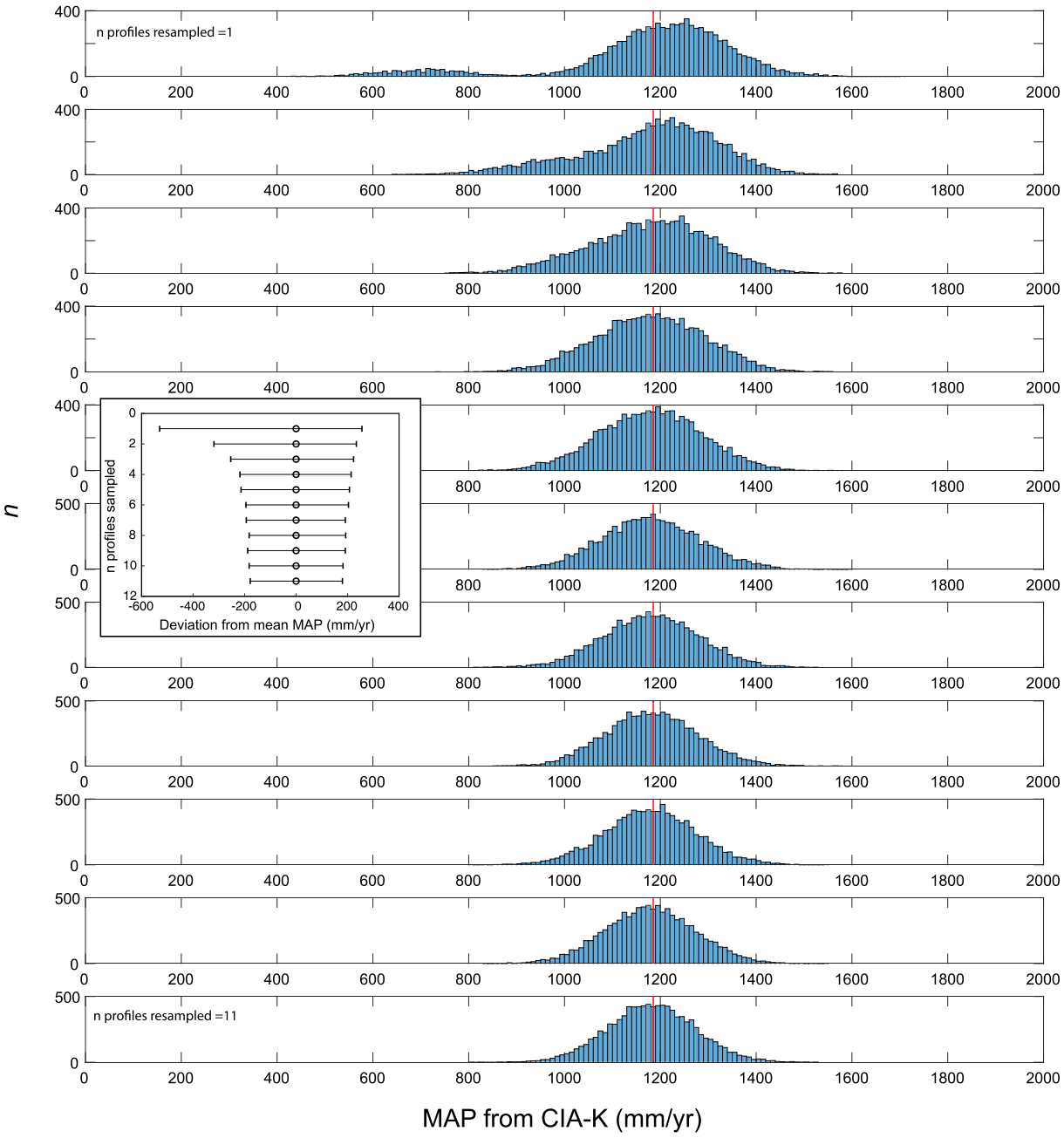

Fig. 7. Resampling results for JMH transect (B horizons with CaO <5%). From top to bottom, the number of profiles included in the resample increases by one (i.e., top panel resamples one profile, bottom panel resamples all 11 profiles). The vertical red line is the average MAP from the dataset. All panels show results from 10,000 trials. The bottom panel effectively represents the mean ± standard error of the regression. (Inset panel) From top to bottom, the deviation from the average MAP value for 1 to 11 profiles resampled, demonstrating how results become more certain with more profiles sampled. (For interpretation of the references to color in this figure legend, the reader is referred to the web version of this article.)

representing the standard error of the distribution about the mean (Fig. 7). At JMH, deviations from the mean (Fig. 7b) show diminishing improvement in MAP variance after more than 4–5 profiles are included, as well as asymmetry in the distribution of resulting MAP values for small numbers of included profiles. These results were repeated in the HB transect, which lacked samples with exceptionally high CaO (Fig. S9). Resampling the JMH profiles with samples exceeding the 5% CaO threshold resulted in a similar result (Fig. S10). There was no discernible difference between the 5% and 11% threshold resampling, as only three samples exceeded the 11% CaO threshold. Resampling for the Kisaaka paleosol, with four profiles but no clear outlier as at JMH, had muted results in a similar pattern, with uncertainty decreasing after two profiles (Fig. S11).

5. Discussion

5.1. Ecosystem and climate reconstruction

Overall, our climatological results agree with proxies from approximately the same geologic time and place. Paleosol-based MAP reconstructions of 1185 ± 182 mm yr^{-1} are comparable to physiognomic reconstructions of the Green River Basin (1160 ± 58 mm yr^{-1}; Wing and Greenwood, 1993), though Wilf et al. (1998) revised this value to be lower, around 840 mm yr^{-1}. MAP and MAAT results are also consistent with penecontemporaneous results from nearby Honeycomb Buttes (~1100 mm yr^{-1}, ~11 °C) (Hyland and Sheldon, 2016). However, later reconstructions of the Honeycomb Buttes paleosols based on clumped

isotope analyses place 11 °C as representative of transitional seasons (e.g., MAM, OND), while the average air temperature from PPM1.0 was higher at 15.2 °C ± 1.3 °C (1σ; Sheldon, 2018). Recent researchers have found that pedogenic carbonates accumulated in B-horizons of soils are not recording mean annual temperature, and instead are seasonally biased (Passey et al., 2010; Quade et al., 2013; Gallagher and Sheldon, 2016; Gallagher et al., 2019a; Gallagher et al., 2019b; Kelson et al., 2020); it would be reasonable to expect that other B horizon processes (e.g., weathering) could be subject to similar seasonal effects.

The proximity to sandy channels, color hues, and presence of hydromorphic soil features (mottling, drab-haloed root traces; lack of carbonate nodules) suggests a frequently wet floodplain environment for these paleo-Inceptisols, with some wet/dry cycles indicated by the presence of slickensides. The Holdridge life-zone designation of wet forest is reasonable in this context, as well as with the proxy-based paleoclimate reconstructions. (The 'wet tundra' designation for Paleosol 4 is driven by high CaO and should not be considered robust.) Ecosystem results based on our data align with findings from nearby ecosystems (e.g., Hyland et al., 2013; Hyland et al., 2018; Stein et al., in prep/review). Paleobotanical evidence from the proximal (in space and time) Bridger Formation includes trees, understory and climbing ferns consistent with subtropical forest conditions (Allen, 2017a, 2017b). Paleocene Eocene Thermal Maximum (PETM) and early Eocene climatic optimum estimates from the Bighorn Basin to the northeast plot as wet forest conditions (Wing et al., 2005; Wing and Currano, 2013), as do early Eocene estimates from the Bridger Formation (e.g., Blue Rim, WY; Allen, 2017a, 2017b; Stein et al., 2021). Although southwest Wyoming today is a cold, dry-scrub/desert, the early Eocene was equable and latitudes as far north as British Columbia have fossil evidence that supports the presence of subtropical species (Greenwood et al., 2005; Smith et al., 2009), so it is reasonable that the area would have been warm, wet, and forested at the time.

5.2. Geochemical variability, Ca effect, and proxies

The primary source of geochemical variability in the JMH transect was Ca, with high-CaO samples decreasing the MAP reconstruction for its paleosol profile (Fig. S12). Otherwise, geochemistry and proxies were relatively consistent, similar to previous work on a shorter (1 km) transect (Hyland and Sheldon, 2016). Because the three studies analyzed several different proxies, had different redox regimes, were different maturity levels, and differed in the degree of CaO variability, it is noteworthy that overall heterogeneity in proxies was low in the transects. New intra-horizon sampling presented here also reflects low heterogeneity. That variations in color do not necessarily reflect statistically significant variations in geochemistry or proxy values is a key and encouraging result.

With Ca being a main source of variability in North American soils (which encompass a wide range of climatic and environmental settings; Fig. S12), screening for Ca prior to reconstructions is critical. In modern soils, the distribution of B horizon geochemistry suggests that most soils have <5% CaO (Table S4; Fig. S2). If a paleosol exceeds that value, care should be taken to check for diagenesis or other secondary alteration. A site with paleosols exceeding the CaO threshold would be a good situation to consider using relative rather than quantitative change. Because most proxies (except CALMAG, which has an upper threshold of 10% CaO; Nordt and Driese, 2010) were developed on noncalcareous or weakly calcareous parent materials, future work should develop more proxies for carbonate-parented non-Vertic soils.

Profiles in different redox regimes yield similar paleoclimate results, suggesting that while redox variation indicates small-scale hydrology, paleoclimate results remain robust. One redox-indicator trace element, Mn (e.g., Driese and Sim, 1995), correlates strongly to CaO content in B horizons ($r^2 = 0.95$, $p < 0.001$, $n = 90$; Fig. S6a). Mn was more variable in the JMH transect than in either the HB or Kisaaka transects. Other redox indicators explored (Fe, Cr) had less linear negative correlations with CaO (Fig. S6b,c; $r^2 = 0.21$, $p < 0.001$ and $r^2 = 0.48$, $p < 0.001$, $n = 90$ for both). The strong correlation between Mn and CaO could be indicative of Ca– Mn replacement in dispersed carbonates or exchangeable clays during periods in which the paleosol was waterlogged and the redox regime became strongly reducing. The suggested Mn—Ca relationship could be a fruitful path of investigation in future work, and given long-standing interest in paleosol Fe (e.g., Sheldon et al., 2021) and Cr (e.g., Colwyn et al., 2019) as redox indicators in geologic history, the weaker relationships identified here may also be worth further investigation.

Time and weathering intensity are two soil-forming factors which are important to consider. As a soil evolves from an immature or weakly-weathered stage (i.e., Entisol/Inceptisol) to a more mature or intensely-weathered stage (i.e., Alfisol, Ultisol), there could be a systemic change in geochemical variability. By applying a random resampling analysis to transects with Inceptisols, Alfisols, and Vertisols, respectively, we demonstrate that this basic principle of outcrop extent-based sampling uncertainty applies to a variety of soil orders and maturity levels. Future research could improve on this work by resampling in an expanded range of soil orders, as well as more varied environments; JMH and HB effectively represent the same wet forested biome, and the Kisaaka paleosol formed in a tropical savanna (Beverly et al., 2015, 2017). Future work could also explore more explicitly the effect of time or paleosol maturity (i.e., from Entisol to Ultisol), as well as vegetative cover type (e.g., grasslands/paleo-Mollisols), on tendencies for geochemical heterogeneity and proxy uncertainty.

The resampling results highlight the benefits of including more profiles from a single horizon, including increased confidence that sampled profiles are in fact representative of the entire horizon, as well as decreased uncertainty in the absolute proxy outputs. Increasing the number of profiles included narrows the resulting distribution of possible MAP values, but with diminishing impact after 4–5 profiles (Fig. 7b). The distribution begins to converge around 4–5 profiles for our JMH site, with limited 'return on investment' of including more profiles beyond that point (Fig. 7b). Similarly, HB begins to converge at 3–4 profiles sampled because it has less geochemical variability (Fig. S9). The Kisaaka paleosol is more difficult to compare at 1.5 km with 4 profiles, but it still shows the decrease in uncertainty at 3 profiles (Fig. S11). Practically as well as logically, then, sampling at least three profiles for a transect of any extent is a robust baseline practice. Beyond that point, the number of profiles that should be sampled scales with extent and the apparent degree of variability.

5.3. Paleosols as stratigraphic markers

Kraus and colleagues identified early on paleosols' strengths and shortcomings as recorders of environment and placemarkers in basin-wide stratigraphy. Considering spatial (horizontal) as well as temporal (vertical) distribution variability in paleosols is important to be able to best use paleosols in interpreting basin-scale changes in hydrology and environment, as well as using them as relative markers. Relying on a paleosol designation from a single profile, or from multiple profiles closely grouped together within a basin, for basin-wide or regional correlation should be done carefully, given that — as with modern soils — relatively small changes in topography, biosphere, and hydrology can affect both the type of paleosol and whether or not it would be preserved at all. It is common for a basin to have multiple pedotypes present, with their particular distribution dependent in part on basin-wide fluvial processes (e.g., Kraus, 1999; Tabor et al., 2006; Hamer et al., 2007; Rosenau et al., 2013a, 2013b; Weissmann et al., 2013).

Many paleosol studies effectively examine vertical/temporal variability when looking at paleosol sequences through time, but it is imperative to understand the geochemical variability *within* a paleosol—both internally and laterally—so we can know if the temporal changes are within error, essentially, of the lateral distribution, or if the observed/reconstructed changes are larger and therefore significant,

representing meaningful, actual change in climate or environment. Additionally, interpreting a paleosol accurately depends on understanding its paleotopographic context, which can only be done through examining its lateral extent (Adams et al., 2011). More broadly, to most accurately interpret a paleosol, its position in a basin-wide context should be known (e.g., proximal, distal, different inputs; Kraus, 1987; Bown and Kraus, 1987; Kraus, 1999), and the preservation bias for flat or low-lying floodplains should be considered.

Paleosols are useful chemostratigraphic indicators because of their distinctive weathering patterns that become particularly evident in stacked paleosol successions (Kraus, 1999). By tracking vertical/temporal changes in multiple geochemical proxies/weathering indices (e.g., CIA, isotopic changes, provenance indicators), such successions have been used to track global shifts in climate on a basin-wide scale (e.g., Sheldon and Retallack, 2004; Baczynski et al., 2013; Hyland et al., 2017). These relative changes in weathering should be consistent throughout the basin if similar paleosols/pedotypes are compared (i.e., similar pedofacies and order), but correlations could fail if the basin has tectonic/sedimentary regimes that are substantially different at one end from the other. Like other climate-change tools, chemostratigraphic tools are best used in conjunction with other dating and relative stratigraphic markers.

Under-sampling a paleosol weakens its physiochemical description (making it harder to correlate across larger scales) and limits certainty of paleoclimate/paleoenvironmental proxies. The contributions in this work towards improving paleoclimate proxy uncertainty primarily improve paleosols' use as chemostratigraphic markers in vertical sections because at basin or larger scales, it is often unlikely that a single paleosol transect would be present uninterrupted. By refining an approach to proxy uncertainty, the chemostratigraphic marker becomes better defined. Sampling fewer profiles in building a chemostratigraphic record minimizes the ability to confidently correlate trends in paleoclimate proxies across regional scales. Sampling fewer profiles in a well-defined transect could also lead to erroneous interpretations of climatic or environmental change when the observed variability is, in fact, due to synchronous variability. Redox variability in the physical appearance of paleosols in the JMH transect serves as an example of this.

5.4. Implications for uncertainty and analyses

Because both JMH and HB had relatively consistent geochemistry and a clear climate signal, our findings support the use of paleosol-based proxies—with the important caveat that sampling multiple profiles affects reconstruction uncertainty. Sampling a single paleosol profile, even with multiple samples per horizon within that profile, does not provide sufficient information on how representative of the whole paleosol extent, let alone the landscape-scale, that profile might be. Our resampling exercise demonstrates that without considering the uncertainty associated with outcrop limitations, paleosol-based reconstructions are falsely precise, perhaps leading to overinterpretation of individual outcrops or in the context of time-series changes (i.e., climate change). It is particularly important to consider as many sources of uncertainty/variability as possible when taking reconstructions a step further (e.g., to paleoaltimetry), as any unaccounted-for uncertainty could compound in the next level of work.

Based on our results, paleosol reconstructions that do not incorporate outcrop-based uncertainty may have over-interpreted the significance of apparent climate change based on paleosol geochemical proxies. That is, without quantifying the true lateral variability of an outcrop, we cannot definitively say whether there has been significant temporal change unless it greatly exceeds the proxy calibration error. By increasing the lateral and/or vertical sampling coverage, we can address this uncertainty. It could also be prudent to think in terms of relative, rather than absolute/quantitative, changes for outcrops with limited extent, both in terms of magnitude and climate/environment. This more conservative approach still allows interpreting large-scale climate and environmental shifts that we're interested in and that could be linked to broader/global trends, as is currently the case with global chemostratigraphic correlations in carbon cycle disturbances/the C isotope record (Sahy et al., 2015; Cotton et al., 2015; Gallagher et al., 2019a; Gallagher et al., 2019b). Relative changes in weathering in paleosol successions have been used (e.g., Sheldon et al., 2012; Hyland et al., 2013), but this is not common practice. At the least, relative changes should be considered along with quantitative changes, and in the context of both proxy- and outcrop-based uncertainties. For profiles and outcrops with limited lateral sampling opportunities (and therefore lower confidence in their representativeness), we encourage placing more weight on relative changes than absolute values.

Finally, we note that paleosols' lateral geochemical variability could influence local taphonomy. For example, mesoscale topographic changes can influence plant growth, water ponding, and redox state, which together can influence preservation likelihood (e.g., Demko et al., 1998; Trueman, 1999; Behrensmeyer et al., 2000; Gastaldo and Demko, 2010). Little work has been done on paleosol geochemical variability and taphonomy, and what potential biases this introduces into terrestrial paleobotanical/palynological records (e.g., Hyland, 2014) or to studies that seek to “fingerprint” fossil remains by comparing their chemistry to the paleosol chemistry (e.g., Metzger et al., 2004). This area merits further investigation.

5.5. Implications for fieldwork

Outcrop limitations are the foremost constraint on paleosol fieldwork. A single, small outcrop is statistically not that informative unless coupled with other nearby outcrops; this may limit the number of sites where we can do paleosol-based reconstructions, but it is necessary to acknowledge this fundamental constraint. Rather than being prescriptive, this resampling exercise generally demonstrates the uncertainty inherent in using a single paleosol profile to represent a landscape rather than a lateral outcrop. Practically, there is no set number of paleosol profiles that should be sampled per some given distance. At a minimum, three paleosol profiles should be sampled for basic repeatability testing, ideally with multiple samples from within each horizon to constrain any internal variability (i.e., Ca hotspots). Beyond that, the number of profiles to sample essentially scales with extent and degree of apparent variability. An additional ‘best practice’ is to report outcrop lateral extents (in addition to profiles' vertical thickness), along with the variability in their exposure quality and features.

When determining how many profiles to sample either vertically or laterally, it is crucial to consider the needs and limitations of the relevant scientific questions. Defining a transition from a forest to a desert over a 5 my record requires a lower-resolution record than capturing a smaller-magnitude shift in climate. The latter case, then, also calls for a better description of the uncertainty in paleoclimate proxies than in the former. Nuanced changes in climate (e.g., a change in MAP of 200 mm yr^{-1}) is more defensible with robust sampling that allows a well-defined range of uncertainty. Quantitative proxy changes that far exceed calibration errors can be confidently interpreted as change; when the change is smaller in magnitude, a more conservative interpretation may be more appropriate.

6. Conclusions

The primary conclusion from this work is that sampling strategy affects the uncertainty on paleosol-based proxies, and that uncertainty should be taken into account both when planning sampling/fieldwork and analyzing paleoclimate reconstruction data. In general, as we constrain different types of uncertainty around paleosol-based proxies that are currently underestimated or not accounted for, we should be more conservative in interpreting paleoclimate reconstructions as absolute. Relying solely on calibration-based fixed standard error underestimates the true uncertainty of the reconstructed value; until these

other sources of error are incorporated into reconstructions, we recommend analyzing relative changes, particularly for shorter timescale or higher-resolution datasets with relatively few profiles sampled.

This study lays the groundwork for improving the statistical uncertainty on paleosol-based proxies that stems from lateral variability and the hurdles to reliably scaling single outcrop-based reconstructions to basin-wide and regional scales. Carrying out more multiple km-scale transect analyses, such as the work presented here, would improve our understanding of these uncertainty effects in a range of environments and soil orders. Ideally, the community will work towards having multiple such transects from single large basins, like the Green River Basin, that record critical transition periods in Earth's history. Including varied data (e.g., regular and clumped isotopes, phytoliths, mineralogical indicators such as Goethite/Hematite) could improve understanding of how different terrestrial biogeochemical processes are linked at landscape scales, and how their different preservation biases could affect our interpretation of their records. Finally, carrying out these statistical analyses in a variety of soil orders and environments would make landscape-scale paleoclimate and paleoenvironmental reconstructions more robust.

Declaration of Competing Interest

The authors declare no conflicts of interest.

Acknowledgements

This work funded by NSF Award #1812949 to N. Sheldon and others. Thanks to B. Gallina and S.M. Vogel for assistance with sample preparation and Munsell color identification in the lab.

Appendix A. Supplementary data

Supplementary data to this article can be found online at https://doi.org/10.1016/j.palaeo.2021.110641.

References

Adams, J.S., Kraus, M.J., Wing, S.L., 2011. Evaluating the use of weathering indices for determining mean annual precipitation in the ancient stratigraphic record. Palaeogeogr. Palaeoclimatol. Palaeoecol. 309, 358–366.
Allen, S.E., 2017a. Reconstructing the local vegetation and seasonality of the lower Eocene Blue Rim site of southwestern Wyoming using fossil wood. Int. J. Plant Sci. 178, 689–714.
Allen, S.E., 2017b. The Uppermost Lower Eocene Blue Rim Flora from the Bridger Formation of Southwestern Wyoming: Floristic Composition, Paleoclimate, and Paleoecology. Doctoral Dissertation. University of Florida.
Baczynski, A.A., McInerney, F.A., Wing, S.L., Kraus, M.J., Block, J.I., Boyer, D.M., Secord, R., Morse, P.E., Fricke, H.C., 2013. Chemostratigraphic implications of spatial variation in the Paleocene-Eocene Thermal Maximum carbon isotope excursion, SE Bighorn Basin, Wyoming. Geochem. Geophys. Geosyst. 14, 4133–4152.
Behrensmeyer, A.K., Kidwell, S.M., Gastaldo, R.A., 2000. Taphonomy and paleobiology. Paleobiology 26, 103–147.
Beverly, E.J., Driese, S.G., Peppe, D.J., Arellano, L.N., Blegen, N., Faith, J.T., Tryon, C.A., 2015. Reconstruction of a semi-arid late Pleistocene paleocatena from the Lake Victoria region, Kenya. Quat. Res. 84, 368–381.
Beverly, E.J., Peppe, D.J., Driese, S.G., Blegen, N., Faith, J.T., Tryon, C.A., Stinchcomb, G.J., 2017. Reconstruction of late Pleistocene paleoenvironments using bulk geochemistry of paleosols from the Lake Victoria region. Front. Earth Sci. 368–381.
Bown, T.M., Kraus, M.J., 1987. Integration of channel and floodplain suites. I. Developmental sequence and lateral relations of alluvial paleosols. J. Sediment. Petrol. 57, 587–601.
Brantley, S.L., Goldhaber, M.B., Ragnarsdottir, K.V., 2007. Crossing disciplines and scales to understand the critical zone. Elements 3, 307–314.
Braunagel, L.H., Stanley, K.O., 1977. Origin of variegated redbeds in the Cathedral Bluffs tongue of the Wasatch Formation (Eocene), Wyoming. J. Sediment. Res. 47, 1201–1219.
Breecker, D.O., 2013. Quantifying and understanding the uncertainty of atmospheric CO_2 concentrations determined from calcic paleosols. Geochem. Geophys. Geosyst. 14, 3210–3220.
Cerling, T.E., 1984. The stable isotopic composition of modern soil carbonate and its relationship to climate. Earth Planet. Sci. Lett. 71, 229–240.
Chetel, L.M., Carroll, A.R., 2010. Terminal infill of Eocene Lake Gosiute, Wyoming, U.S.A. J. Sediment. Res. 80, 492–514.
Clyde, W.C., Zonnevold, J.P., Stamatakos, J., Gunnel, G.F., Bartels, W.S., 1997. Magnetostratigraphy across the Wasatchian/Bridgerian NALMA boundary (Early to Middle Eocene) in the Western Green River Basin, Wyoming. J. Geol. 105, 657–669.
Clyde, W.C., Sheldon, N.D., Koch, P.L., Gunnell, G.F., Bartels, W.S., 2001. Linking the Wasatchian/Bridgerian boundary to the Cenozoic Global climate Optimum: new magnetostratigraphic and isotopic results from South Pass, Wyoming. Palaeogeogr. Palaeoclimatol. Palaeoecol. 167, 175–199.
Colwyn, D.A., Sheldon, N.D., Maynard, J.B., Gaines, R., Hofmann, A., Wang, X., Gueguen, B., Asael, D., Reinhard, C.T., Planavsky, N.J., 2019. A paleosol record of the evolution of Cr redox cycling and evidence for an increase in atmospheric oxygen during the Neoproterozoic. Geobiology 17, 579–593.
Cotton, J.M., Sheldon, N.D., Hren, M.T., Gallagher, T.M., 2015. Positive feedback drives carbon release from soils to atmosphere during Paleocene/Eocene warming. Am. J. Sci. 315, 337–361.
Demko, T.M., Dubiel, R.F., Parrish, J.T., 1998. Plant taphonomy in incised valleys: implications for interesting paleoclimate from fossil plants. Geology 26 (12), 1119–1122.
Driese, S.G., Ashley, G.M., 2016. Paleoenvironmental reconstruction of a paleosol catena, the Zinj archaeological level, Olduvai Gorge, Tanzania. Quat. Res. 85, 133–146.
Driese, S.G., Sim, E.L., 1995. Redoximorphic paleosols in alluvial and lacustrine deposits, 1.8Ga Lochness Formation, Mount Isa, Australia: Pedogenic processes and implications for paleoclimate. J. Sediment. Res. 65A, 675–689.
Dzombak, R.M., Sheldon, N.D., 2020. Weathering intensity and presence of vegetation are key controls on soil phosphorus concentrations: implications for past and future terrestrial ecosystems. Soil Syst. 4, 73. https://doi.org/10.3390/soilsystems4040073.
Fedo, C.M., Nesbitt, H.W., Young, G.M., 1995. Unraveling the effects of potassium metasomatism in sedimentary rocks and paleosols, with implications for paleoweathering conditions and provenance. Geology 23, 921–924.
Fricke, H.C., Wing, S.L., 2004. Oxygen isotope and paleobotanical estimates of temperature and $\delta^{18}O$–latitude gradients over North America during the early Eocene. Am. J. Sci. 304, 612–635.
Gallagher, T.M., Sheldon, N.D., 2013. A new paleothermometer for forest paleosols and its implications for Cenozoic climate. Geology 41, 647–650.
Gallagher, T.M., Sheldon, N.D., 2016. Combining soil water balance and clumped isotopes to understand the nature and timing of pedogenic carbonate formation. Chem. Geol. 435, 79–91.
Gallagher, T.M., Cacciatore, C.G., Breecker, D.O., 2019a. Interpreting the difference in magnitudes of PETM carbon isotope excursions in paleosol carbonate and organic matter: oxidation of methane in soils versus elevated soil respiration rates. Palaeoceanogr. Paleoclimatol. 34, 2113–2128.
Gallagher, T.M., Hren, M., Sheldon, N.D., 2019b. The effect of soil temperature seasonality on climate reconstructions from paleosols. Am. J. Sci. 319, 549–581.
Gastaldo, R.A., Demko, T.M., 2010. The relationship between continental landscape evolution and the plant-fossil record: Long term hydrologic controls on preservation. Chapter in: Taphonomy, pp 249–285. In: Aims & Scope Topics in Geobiology Book Series, Volume 32. Springer.
Greenwood, D.R., Archibald, S.B., Matthews, R.W., Moss, P.T., 2005. Fossil biotas from the Okanagan Highlands, southern British Columbia and northeastern Washington State: climates and ecosystems across an Eocene landscape. Can. J. Earth Sci. 42, 167–185.
Gulbranson, E.L., Montanez, I.P., Tabor, N.J., 2011. A proxy for humidity and floral province form paleosols. J. Geol. 119, 559–573.
Hamer, J.M.M., Sheldon, N.H., Nichols, G.J., Collinson, M.E., 2007. Late Oligocene-Early Miocene paleosols of distal fluvial systems, Ebro Basin, Spain. Palaeo 247, 220–235.
Harnois, 1988. CIW (CIA-K) the CIW Index: a new chemical index of weathering. Sediment. Geol. 55 (1988), 319–322.
Holdridge, L.R., 1947. Determinations of world plant formations from simple climatic data. Science 105, 367–368.
Hyland, E.G., 2014. Phytoliths as tracers of recent environmental change. In: Chapter in Experimental Approaches to Understanding Fossil Organisms. Springer, UK, pp. 207–225.
Hyland, E.G., Sheldon, N.D., 2013. Coupled CO_2-climate response during the early Eocene climatic optimum. Palaeogeogr. Palaeoclimatol. Palaeoecol. 369, 125–135.
Hyland, E.G., Sheldon, N.D., 2016. Examining the spatial consistency of palaeosol proxies: implications for palaeoclimatic and palaeoenvironmental reconstructions in terrestrial sedimentary basins. Sedimentology 63, 959–971.
Hyland, E.G., Sheldon, N.D., Cotton, J.M., 2017. Constraining the early Eocene climatic optimum: a terrestrial interhemispheric comparison. GSA Bull. 129, 244–252.
Hyland, E.G., Huntington, K.W., Sheldon, N.D., Reichgelt, T., 2018. Temperature seasonality in the north American continental interior during the early Eocene Climatic Optimum. Clim. Past 14, 1391–1404.
Jenny, H.J., 1941. Factors in Soil Formation. McGraw-Hill, New York, NY, USA.
Kelson, J.R., Huntington, K.W., Breecker, D.O., Burgener, L.K., Gallagher, T.M., Hoke, G. D., Petersen, S.V., 2020. A proxy for all seasons? A synthesis of clumped isotope data from Holocene soil carbonates. Quat. Sci. Rev. 234, 106259.
Kraus, M.J., 1987. Integration of channel and floodplain suites, II. Vertical relations of alluvial paleosols. J. Sed. Petrology 57, 602–612.
Kraus, M.J., 1997. Lower Eocene alluvial paleosols: pedogenic development, stratigraphic relationships, and paleosol-landscape association. Palaeogeogr. Palaeoclimatol. Palaeoecol. 129 (1997), 387–406.
Kraus, M.J., 1999. Paleosols in clastic sedimentary rocks: their geologic applications. Earth Sci. Rev. 47, 41–70.

Lugo, A.E., Brown, S.L., Dodson, R., Smith, T.S., Shugart, H.H., 1999. The Holdridge life zones of the conterminous United States in relation to ecosystem mapping. J. Biogeogr. 26, 1025–1038.
Lukens, W.E., Stinchcomb, G.E., Nordt, L.C., Kahle, D.J., Driese, S.G., Tubbs, J.D., 2019. Recursive partitioning improves paleosol proxies for rainfall. Am. J. Sci. 319, 819–845.
Mack, G.H., James, W.C., Monger, H.C., 1993. Classification of paleosols. Geol. Soc. Am. Bull. 105, 129–136.
Marbut, C.F., 1935. Atlas of American Agriculture. III. Soils of the United States. Government Printing Office, Washington, D.C.
Maynard, J.B., 1992. Chemistry of modern soils as a guide to interpreting precambrian paleosols. J. Geol. 100, 279–289.
Mederos, S., Tikoss, B., Bankey, V., 2005. Geometry, timing, and continuity of the Rock Springs uplift, Wyoming, and Douglas Creek arch, Colorado: implications for uplift mechanisms in the Rocky Mountain foreland, U.S.A. Rocky Mountain Geol. 40, 167–191.
Metzger, C.A., Terry Jr., D.O., Grandstaff, D.E., 2004. Effect of paleosol formation on rare earth element signatures in fossil bone. Geology 32, 497–500.
Michel, L.A., Tabor, N.J., Montanez, I.P., 2016. Paleosol diagenesis and its deep-time paleoenvironmental implications, Pennsylvanian-Permian Lodève Basin, France. J. Sediment. Res. 86, 813–829.
Michel, L.A., Sheldon, N.D., Myers, T.S., Tabor, N.J., 2021. Assessment of pretreatment methods on CIA-K and CALMAG indices and the effects on paleoprecipitation estimates. Palaeogeogr. Palaeoclimatol. Palaeoecol.
Nordt, L.C., Driese, S.D., 2010. New weathering index improves paleorainfall estimates from Vertisols. Geology 38 (2010), 407–410.
Nordt, L.C., Driese, S.G., 2014. Application of the critical zone concept to the deep-time sedimentary record. Sediment. Record 11, 4–9.
Passey, B.H., Levin, N.E., Cerling, T.E., Brown, F.H., Eiler, J.M., 2010. High-temperature environments of human evolution in East Africa based on bond ordering in paleosol carbonates. Proc. Natl. Acad. Sci. 107, 11245–11249.
Prochnow, S.J., Nordt, L.C., Atchley, S.C., Hudec, M.R., 2006. Multi-proxy paleosol evidence for middle and late Triassic cliamte trends in eastern Utah. Palaeo3 232 (1), 53–72.
Quade, J., Eiler, J., Daeron, M., Achyuthan, H., 2013. The clumped isotope geothermometer in soil and paleosol carbonate. Geochim. Et Cosmochim. Acta 105, 92–107.
Rasmussen, C., Tabor, N.J., 2007. Applying a quantitative pedogenic energy model across a range of environmental gradients. Soil Sci. Soc. Am. J. 71, 1719–1729.
Rasmussen, C., Southard, R.J., Horwath, W.R., 2005. Modeling energy inputs to predict pedogenic environments using regional environmental databases. Soil Sci. Soc. Am. J. 69, 1266–1274.
Retallack, G.J., 1991. Untangling the effects of burial alteration and ancient soil formation. Annu. Rev. Earth Planet. Sci. 19, 183–206.
Retallack, G.J., 2001. Soils of the Past. Blackwell, Oxford, p. 600.
Retallack, G.J., 2005. Pedogenic carbonate proxies for amount and seasonality of precipitation in paleosols. Geology 33, 333–336.
Rosenau, N.A., Tabor, N.J., Elrick, S.D., Nelson, W.J., 2013a. Polygenetic history of paleosols in Middle-Upper Pennsylvanian cyclothems of the Illinois Basin, USA. Part I: Characterization of paleosol types and interpretations of pedogenic processes. J. Sediment. Res. 83, 606–636.
Rosenau, N.A., Tabor, N.J., Elrick, S.D., Nelson, W.J., 2013b. Polygenetic history of paleosols in Middle-Upper Pennsylvanian cyclothems of the Illinois Basin, USA. Part II: the impacts of geomorphology, climate, and glacioeustasy. J. Sediment. Res. 83, 637–668.
Rye, R., Holland, H., 1998. Paleosols and the evolution of atmospheric oxygen: a critical review. Am. J. Sci. 298, 621–672.
Sahy, D., Condon, D.J., Terry Jr., D.O., Fischer, A.U., Kuiper, K.F., 2015. Synchronizing terrestrial and marine records of environmental change across the Eocene-Oligocene transition. Earth Planet. Sci. Lett. 427, 171–182.
Sheldon, N.D., 2006. Quaternary glacial-interglacial climate cycles in Hawaii. J. Geol. 114, 367–376.
Sheldon, N.D., 2018. Using carbonate isotope equilibrium to screen pedogenic carbonate oxygen isotopes: implications for paleoaltimetry and paleotectonic studies. Geofluids, 5975801. https://doi.org/10.1155/2018/5975801.
Sheldon, N.D., Retallack, G.J., 2004. Regional Paleoprecipitation records from the Lake Eocene and Oligocene of North America. J. Geol. 112, 487–494.
Sheldon, N.D., Tabor, N.J., 2009. Quantitative paleoclimatic and paleoenvironmental reconstruction using paleosols. Earth Sci. Rev. 95, 1–52.
Sheldon, N.D., Retallack, G.J., Tanaka, S., 2002. Geochemical climofunctions from north American soils and application to paleosols across the Eocene-Oligocene boundary in Oregon. J. Geol. 110, 687–696.
Sheldon, N.D., Costa, E., Cabrera, L., Garcés, M., 2012. Continental climatic and weathering response to the Eocene-Oligocene transition. J. Geol. 120, 227–236.
Sheldon, N.D., Mitchell, R.L., Dzombak, R.M., 2021. Reconstructing Precambrian pCO_2 and pO_2 Using Paleosols. Cambridge University Press, Cambridge, UK.
Smith, D.B., Cannon, W.F., Woodruff, L.G., Solano, F., Ellefsen, K.J., 2014. Geochemical and Mineralogical Maps for Soils of the Conterminous United States; U.S. Geological Survey Open-File Report. United States Geological Survey, Denver, CO, USA, 386p, (ISSN 2331-1258).
Smith, M.E., Carroll, A.R., Singer, B.S., 2008. Syoptic reconstruction of a major ancient lake system: eocene Green River Formation, western United States. GSA Bull. 120, 54–84.
Smith, R.Y., Basinger, J.F., Greenwood, D.R., 2009. Depositional setting, fossil flora, ad paleoenvironment of the early Eocene Falkland site, Okanagan Highlands, British Columbia. Can. J. Earth Sci. 46, 811–822.
Stein, R.A., Sheldon, N.D., Dzombak, R.M., Smith, M.E., Allen, S.E., 2021. A comprehensive approach to climate & ecology in the Eocene Rocky Mountain Interior. Clim. Past.
Stiles, C.A., Mora, C.I., Driese, S.G., 2001. Pedogenic iron-manganese nodules in Vertisols: a new proxy for paleoprecipitation? Geology 29, 943–946.
Stinchcomb, G.E., Nordt, L.C., Driese, S.G., Lukens, W.E., Williamson, F.C., Tubbs, J.D., 2016. A data-driven spline model designed to predict paleoclimate using paleosol geochemistry. Am. J. Sci. 316, 746–777.
Sutherland, W.M., Luhr, S.C., 2011. Preliminary bedrock geologic map of the Farson 30' x 60' quadrangle, Sweetwater, Sublette and Fremont Counties, Wyoming. Wyoming State Geological Survey. 1:100,000. Accessible online at. https://ngmdb.usgs.gov/Prodesc/proddesc_95798.htm.
Tabor, N.J., Myers, T.S., 2015. Paleosols as indicators of paleoenvironment and paleoclimate. Ann. Rev. Earth and Planetary Sci. 43, 333–361.
Tabor, N.J., Montanez, I.P., Kelso, K.A., Currie, B., Shipman, T., Colombi, C., 2006. A late Triassic soil catena: landscape and climate controls on paleosol morphology and chemistry across the Carnian-age Ischigualasto-Villa Union basin, northwestern Argentina. Geol. Soc. Am. Spec. Pap. 416, 17–41.
Tabor, N.J., Myers, T.S., Gulbranson, E., Rasmussen, C., Sheldon, N.D., Carbon stable isotope composition of modern calcareous soil profiles in California: implications for CO2 reconstructions from calcareous paleosols, in, 2013. In: Driese,, S.G., Nordt, L.C. (Eds.), New Frontiers in Paleopedology and Terrestrial Paleoclimatology, SEPM Special Publication No., 104, pp. 17–34. https://doi.org/10.2110/sepmsp.104.07.
Tabor, N.J., Sidor, C.A., Smith, R.M.H., Nesbitt, S.J., Angielczyk, K.D., 2017. Paleosols of the Permian-Triassic: proxies for rainfall, climate change, and major changes in terrestrial tetrapod diversity. Journal of Vertebrate Paleontology 37, 240–253. https://doi.org/10.1080/02724634.2017.1415211.
Trueman, C.N., 1999. Rare earth element geochemistry and taphonomy of terrestrial vertebrate assemblages. Palaios 14, 555–568.
Weissmann, G.S., Hartley, A.J., Scuderi, L.A., Nichols, G.J., Davidson, S.K., Own, A., Atchley, S.C., Bhattacharyya, P., Chakraborty, T., Ghosh, P., Nordt, L.C., Michel, L., Tabor, N.J., 2013. Prograding distributive fluvial systems–geomorphic models and ancient examples. In: Chapter in New Frontiers in Paleoped. And Terrestrial Paleoclimatology, pp. 131–147. Tulsa, OK, USA.
Wilf, P., 2000. Late Paleocene–early Eocene climate changes in southwestern Wyoming: paleobotanical analysis. Geol. Soc. Am. Bull. 112, 292–307.
Wilf, P., Wing, S.L., Greenwood, D.R., Greenwood, C.L., 1998. Using fossil leaves as paleoprecipitation indicators: an Eocene example. Geology 26, 203–206.
Wing, S.L., Currano, E.D., 2013. Plant response to a global greenhouse event 56 million years ago. Am. J. Bot. 100, 1234–1254.
Wing, S.L., Greenwood, D.R., 1993. Fossils and fossil climate: the case for equable continental interiors in the Eocene. Philos. Trans. R. Soc. Lond. Ser. B Biol. Sci. 341, 243–252.
Wing, S.L., Harrington, G.J., Smith, F.A., Bloch, J.I., Boyer, D.M., Freeman, K.H., 2005. Transient floral change and rapid global warming at the Paleocene-Eocene boundary. Science 310, 993–996.